Supporting Information

for

Synthesis and characterization of ionic block copolymer templated calcium phosphate nanocomposites

M. Kanapathipillai, Y.Yusufoglu, A. Rawal, Y.-Y. Hu, C.-T. Lo, P. Thiyagarajan, Y.E. Kalay, M. Akinc, S. Mallapragada, K. Schmidt-Rohr

This Supporting Information provides details on the experimental techniques and associated sample preparation, as well as basic materials characterization including differential scanning calorimetry and thermogravimetry. It also presents dynamic mechanical analysis of the gels. Further, it shows additional two-dimensional ^{31}P-^{1}H NMR spectra, discusses the length scale probed in ^{1}H spin diffusion NMR, and displays additional electron micrographs of the nanocomposites. References additional to those in the main text are given at the end.

Pentablock copolymer characterization. NMR and GPC measurements were performed to determine the composition and molecular weights of the block copolymers. All ^{1}H NMR measurements were performed using a Varian VXR400 (400 MHz) spectrometer, in D_2O and chloroform-d solvents. Molecular weight and polydispersity index (PDI) of the copolymers were estimated using four PLgel columns 100, 500, $1x10^4$, $1x10^5$ Å from Polymer Laboratories at 40° C equipped with a Waters 510 pump, Waters 717 autosampler, a Wyatt Optilab DSP refractometer, and a Wyatt Dawn EOS light scattering detector. Aqueous solutions of the polymers at various concentrations were prepared in 1mM tris-HCl. Simple tube inversion was used to find the gelation temperature. Titration measurements were carried out to find the pK_a and iep values, and differential scanning calorimetry (DSC) was used to find the critical micellization temperatures of the copolymer solutions. The micelle formation in water is an endothermic first-order transition due to the enthalpy of dehydration of the hydrophobic block [29]. Measurements were carried out using a Thermal Analysis DSC instrument Q 20 equipped with an auto sampler. Samples with masses ranging from 5 to 20 mg were heated from -5 to 50°C at a rate of 5°C/min. The data were corrected by sample weight normalization and subtraction of the linear baseline.

Titration measurements were carried out to obtain the degree of ionization. Potentiometric titrations were carried out using a Corning 313 pH/temperature meter at room temperature. Samples were prepared by dissolving 500 mg of polymer in 50 mL nanopure water. In the case of Penta-PZ copolymers, after the complete dissolution of the polymer in water, the solution was

titrated using 1.0 M NaOH. A pH vs [OH^-] concentration plot was obtained and the iep value was obtained from the inflection point. For the anionic pentablock copolymer, the solution pH was first raised to pH 12 by adding 1.0 M NaOH and then back titrated using 1.0 M HCl. The degree of ionization, α, was calculated from the ratio of the net concentration of H^+ ions (C_H-C_{OH}) and COOH groups (C_A) in solution, $\alpha = \frac{(C_H - C_{OH})}{C_A}$. [30]

Methods for Nanocomposite Characterization. Thermogravimetric analysis (TGA) was performed with a Perkin Elmer thermogravimetric analyzer (Perkin Elmer, TGA 7, Downers Grove IL). Approximately 60 mg of the gel sample was placed in a platinum pan and the experiments were performed in a flowing air environment. The program was set to heat up to 50°C, hold at this temperature for 1 min, then heat from 50°C to 120°C at a rate of 5.00°C/min, and finally, heat from 120°C to 600°C at a rate of 10.00°C/min.

Scanning transmission electron microscopy (STEM) images were captured on a JEOL 1200EX II (Japan Electron Optic Laboratories, Peabody, MA) and FEI-Tecnai G^2-F20 (FEI Inc., Hillsboro, Oregon) scanning transmission electron microscope equipped with EDX (EDX Inc., Mahwah, NJ). The former uses a Megaview III digital camera and SIS Pro. Software (Soft Imaging Systems Inc., LLC, Lakewood, CO), the latter a CCD camera and Digital Micrograph Software (Gatan, Pleasanton, CA). Furthermore, high resolution TEM examination was performed using the same FEI-Tecnai G^2 F20 scanning/transmission electron microscope. For the TEM study, the hydrogel samples were diluted to obtain 5.0 weight % polymer solution. Approximately 50 μL of the aqueous sample was placed onto a Formvar coated copper grid and the contents allowed to settle for 1 min. Most of the supernatant was wicked away and 1% phosphotungstic acid (pH ~ 5) was applied for 30 seconds as a negative contrast stain. The grid was wicked and allowed to dry.

Wide-angle X-ray diffraction patterns were obtained using a theta-theta x-ray diffractometer (Scintag, XDS-2000, Cupertino, CA) operating at 45 kV and 40 mA, and the scanning rate was 0.60°/min with a sampling interval of 0.02° over a range of $10 \leq 2\theta \leq 60°$. To minimize drying, hydrogel XRD samples were prepared and analyzed immediately. Scintag DMSNT search / match software and the ICDD database were used for the phase analysis.

SAXS measurements were performed at the 12-ID beam line at the Advanced Photon Source in Argonne National Laboratory. We used 1 mm thick samples of the gels sandwiched between 25 micron thick Kapton tapes. X-rays with an energy of 12 keV (λ = 1.035 Å) and a 15 x 15 cm^2 mosaic Mar CCD at a sample to detector distance of 2 m were used to measure the

scattered intensity and a pin diode on the beam stop to measure the transmitted beam intensity. For each sample we collected five 1 s exposures and the collected 2D data were corrected and azimuthally averaged to obtain I(Q) data, where $Q = 4\pi \sin\theta/\lambda$ with the scattering angle 2θ and the wavelength λ of the X-rays.

SANS measurements were carried out using the time-of-flight small-angle neutron diffractometer (SAND) at IPNS at Argonne National Laboratory. The SAND instrument provides data in the Q range of 0.004-0.5 $Å^{-1}$ in a single measurement by using a 40x40 cm^2 position-sensitive ^3He detector and neutrons with wavelengths in the range of 1.5-14 Å. The neat polymer gel samples of PentaPZ46-5, PentaPAA27-5, PentaPAA36-5 and the corresponding nanocomposite gel samples were prepared in 1m M Tris-HCl at pH 5.5, in D_2O solution. The gel samples were sealed in Suprasil cylindrical cells with 1 mm path length for the SANS measurements. The scattering data were corrected for empty cell scattering, detector sensitivity, and sample transmission. The differential scattering cross section $I(Q)$ was placed on an absolute scale in the units of cm^{-1}.

Solid-state NMR experiments were performed using a Bruker DSX400 spectrometer (Bruker-Biospin, Rheinstetten, Germany) at 400 MHz for ^1H and 162 MHz for ^{31}P. A Bruker 4-mm double-resonance magic-angle spinning (MAS) probehead was used for 6.5-kHz and 7-kHz MAS ^1H-^{31}P NMR experiments. $^{31}P\{^1H\}$ HARDSHIP NMR experiments were performed at 13-kHz MAS with 2.5-mm rotors in a Bruker double-resonance probehead. The 90^o pulse lengths were 5 μs for ^1H and 4 μs for ^{31}P in the 4-mm probe, and 2.5-μs in the 2.5-mm probe for both ^1H and ^{31}P. The direct-polarization experiments, including those with gated recoupling, were carried out with recycle delays of 100 s at 7 kHz MAS. 2D ^1H-^{31}P correlation experiments without homonuclear decoupling, using the wideline separation (WISE) NMR pulse sequence with hypercomplex data acquisition, were carried out with 256 20-μs t_1 increments and 5-s recycle delays. 2D ^1H-^{31}P heteronuclear correlation (HetCor) NMR experiments were carried out with 100 44-μs t_1 increments and 15-s recycle delays. Lee-Goldburg cross polarization (LGCP) was used for polarization transfer from ^1H to ^{31}P in both "WISE" and HetCor experiments with contact times of 0.7 ms and 0.5 ms, respectively. Two-pulse phase-modulation (TPPM) was used for ^1H-^{31}P dipolar decoupling. The hydroxide proton peak at 0.18 ppm and ^{31}P peak at 2.8 ppm in NIST hydroxyapatite were used as secondary chemical shift references to calibrate the ^1H and ^{31}P chemical shifts, respectively. All NMR experiments were carried out at ambient temperature.

Rheological experiments were carried out using an ARES rheometer (TA Instruments, New Castle, Delaware). Polymer gels samples of 46 wt% PentaPZ (Mw 15,000) and 27 wt% Penta-

PAA (Mn 17,538) were used for the study. Parallel plates with diameters of 50 mm and gap of 1.0 mm were used for all samples. All the measurements were performed in dynamic strain controlled (50%) mode at room temperature. Frequency sweeps were carried out with angular frequency varied from 1 rad/s to 0.001 rad/s, and the modulus measurements were recorded.

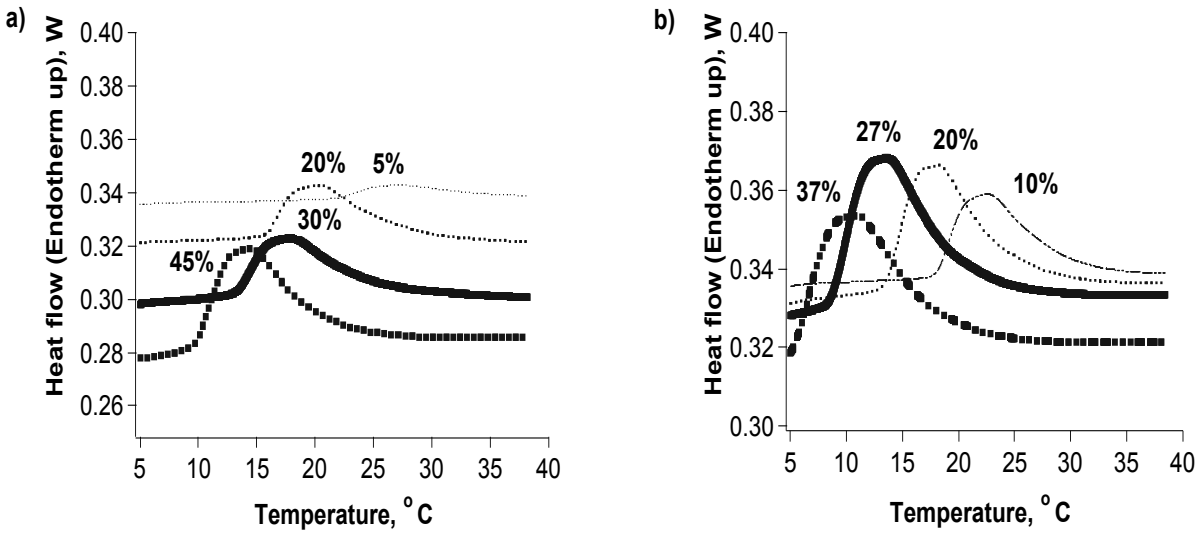

Figure S1. Endothermic micellization peaks of (a) PentaPZ (Mn, 15000) (b) PentaPAA (Mn 17538, PDI-1.196) pentablock copolymers obtained from DSC thermographs.

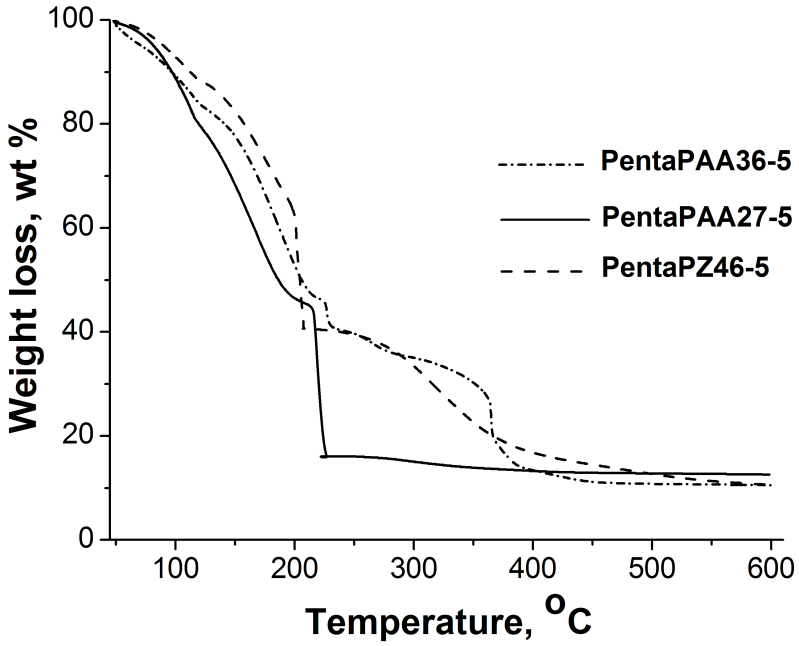

Figure S2. TGA traces of PentaPZ46-5, PentaPAA27-5 and PentaPAA36-5 hydrogels.

Basic materials characterization. Figure S1 shows DSC thermographs of PentaPZ polymers. As

can be seen from the thermograph, critical micellization temperature decreases with increase in concentration. Compared to the zwitteronic pentablock copolymer, the anionic polymer is less ionic. This also can be seen from the DSC thermograph, where the critical micellization temperature is lower for the anionic polymer at similar concentrations.

The TGA curves are shown in Figure S2. The significant weight loss up to 200 ^{o}C is due to the elimination of adsorbed and lattice water. Weight loss observed between 200 - 400 ^{o}C is due to the pyrolysis of the polymer. The origin of the sharp drop in mass at 200-225 ^{o}C is not clear; it has been observed reproducibly in similar samples. The remaining solid after the polymer burn-out is the inorganic phase.

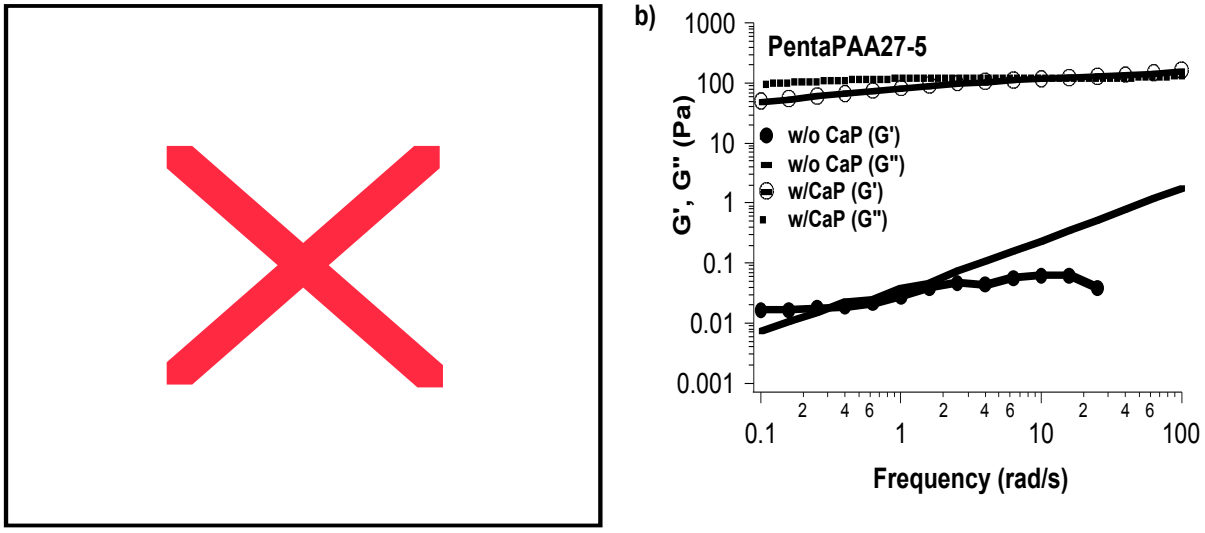

Figure S3. a) Dynamic strain controlled frequency sweep of PentaPZ46-5 and b) PentaPAA27-5 pentablock copolymers with and without calcium phosphate nanocrystals.

Dynamic-mechanical measurements. Dynamic strain controlled rheological measurements were performed on polymer nanocomposite gels to test the stiffness of the formed materials (Figure S3). Measurements indicated an increase in modulus with the inorganic nanocrystals compared to polymer gels alone. The polymer gels alone were not stiff enough due to charge repulsions by the ionic side chains, where the moduli ranged from 0.01-10 Pa. With the formation of the inorganic nanocrystals, the nanocomposites show an increase of modulus by several orders of magnitude depending on the shear rate. Such a large increase may be attributed to neutralization of surface charges on the micelle surface by calcium phosphate phase leading to aggregation of the nanoparticles, or coating of soft polymeric micelles by rigid inorganic particles, or both.

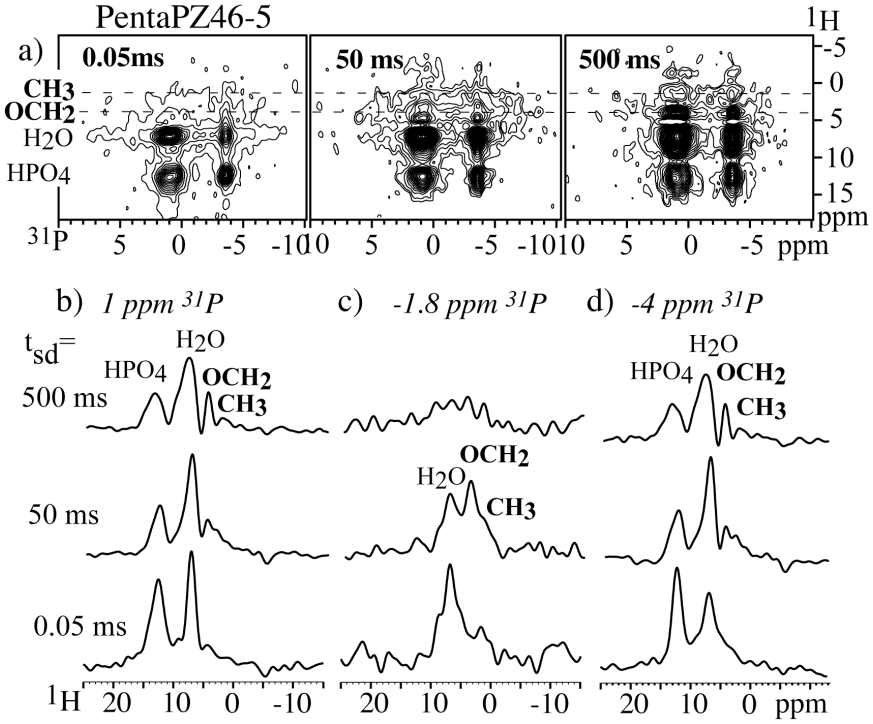

Figure S4. a) 2D ^{1}H-^{31}P HETCOR NMR spectra of PentaPZ46-5 with spin diffusion mixing times of 0.05 ms, 50 ms, and 500 ms. b), c) and d) are cross sections of the 2D spectra at 1.0, -1.8 and -4.0 ppm ^{31}P.

Additional 2D NMR spectra. Figure S4 displays a series of ^{1}H-^{31}P HETCOR spectra of PentaPZ46-5, for spin diffusion times of 0.05, 50, and 500 ms. It shows slow spin diffusion from the polymer to the ^{31}P sites with sharp peaks (Figure S4b,d), but the low broad component centered at –1.8 ppm, which in spite of its low peak height accounts for 66% of the phosphate, exhibits close contact with the polymer (Figure S4c).

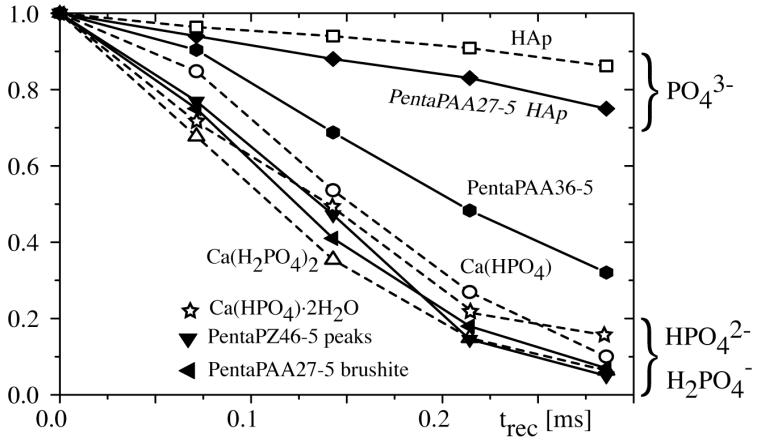

Figure S5. Dephasing of ^{31}P NMR signal under ^{31}P{^{1}H} dipolar recoupling for the polymer—calcium phosphate composites and model compounds. Corresponding spectra for recoupling times of 0 and 2 t_r are shown in Figure 2 of the main text. Spinning frequency: 7 kHz.

^{1}H-^{31}P dephasing curves. Figure S5 shows dephasing of the ^{31}P NMR signal of the

polymer—calcium phosphate composites and model compounds under $^{31}P\{^{1}H\}$ dipolar recoupling for up to two rotation periods, applying a 180° pulse every half rotation period. The faster dephasing of protonated phosphates (HPO_4^{2-}) compared to the unprotonated phosphates (PO_4^{3-}) is clearly seen.

Length scale of ^{1}H spin-diffusion NMR experiments. It is clear that the spin diffusion between different phases occurs the faster the smaller the domains. Thus, it should be possible to convert the time constant of spin diffusion into an estimate of the domain size. The transformation from time constant to length scale is enabled by the spin diffusion coefficient D, which has units of length^2/time. Simple geometric analysis of the initial regime of spin diffusion between two components of equal proton density [32] gives the following relation between the domain size of the dispersed component A and the equilibration time t_{sd}*:

$$d_A = \varepsilon/f_B \, (4/\pi \, D \, t_{sd}^*)^{1/2} \qquad (1)$$

where $f_B = 1 - f_A$ is the proton/volume fraction of component B, and ε is the "dimensionality" of the morphology (ε =1 for lamellar structures, ε =2 for cylinders, and ε = 3 for spheres or other discrete particles). The proton densities and spin diffusion coefficients of the organic and inorganic phases in our samples are not equal, but equation (1) nevertheless provides a basis for domain-size estimates. Reduced ^{1}H linewidths in both organic and inorganic components compared to those of glassy polymers [31,32] allow us to conclude that the effective spin diffusion coefficient will be smaller than 0.4 nm^2/ms. Given that the SAXS experiments discussed below demonstrate that the inorganic phase fills the spaces between the polymer micelles, we should take component A to be the polymer micelles, with ε ~ 3 and a volume/proton fraction of $f_A \sim 0.85$. For $t_{sd}^* = 50$ ms, this gives

$$d_{micelle} < 20 \, (25)^{1/2} \text{ nm} = 100 \text{ nm} \qquad (2)$$

Note that the thickness of the interstitial phosphate layers in this system would be only between 10 and 20 nm. The SAXS and the HARDSHIP NMR data shown below indicate that the RHS of inequality (2) overestimates the true size of the micelles by a factor of six, at least in part due to a significant overestimate of the spin diffusion coefficient and likely also of the equilibration time, which should be obtained by extrapolation of the initial-rate regime of spin diffusion.[32]

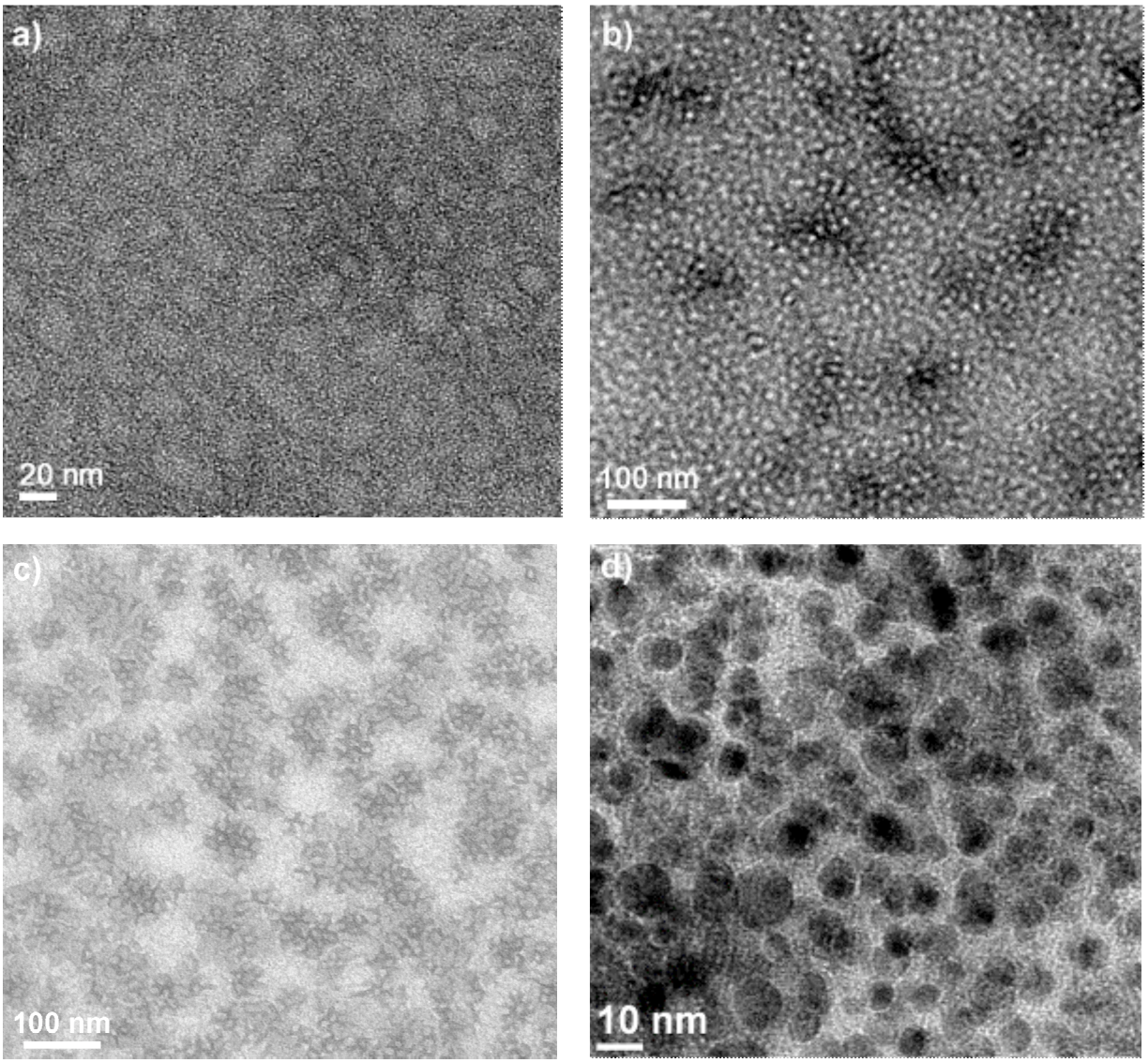

Figure S6. Transmission electron micrographs of stained a) 5 wt% PentaPAA polymer prepared in deionized water, and b) PentaPAA27-5 nanocomposite deposited from a suspension diluted to 5 wt% polymer. Bright spots: unstained polymer. c) PentaPAA36-5 nanocomposite deposited from a suspension diluted to 5 wt% polymer. d) High-angle annular dark field (HAADF) image of diluted PentaPAA27-5 without stain decoration.

Additional electron micrographs. Figure S6 illustrates the micelles in PentaPAA27-5 and PentaPAA36-5. Some of them are surrounded by a calcium phosphate phase, as observed for PentaPAA36-5 in Figure S6c. Spherical black spots in the HAADF image of an unstained sample, Figure S6d, are assigned to the calcium phosphate phase in the polymer. Since the TEM image in Figure S6d was taken without any stain decoration, the polymer micelles are invisible.

Figure S7 show HRTEM images of PentaPAA27-5 and PentaPAA36-5. Calcium phosphate nanoparticles of 5-10 nm size can be clearly seen. The upper and lower insets in Figure S7c show the FFT pattern and filtered inverse-FFT image, respectively. The XRD and NMR

analysis have shown the presence of brushite and hydroxyapatite for PentaPAA27-5. Measurements from several HRTEM images indicated lattice spacings of less than 3.1 Å. An example for this is illustrated in Figure S7c. It shows a lattice spacing of 3.1 Å, which is close to the interplanar spacing of {210} planes for hydroxyapatite and {041} planes for brushite. This makes it difficult to distinguish between brushite and hydroxyapatite phases in PentaPAA27-5.

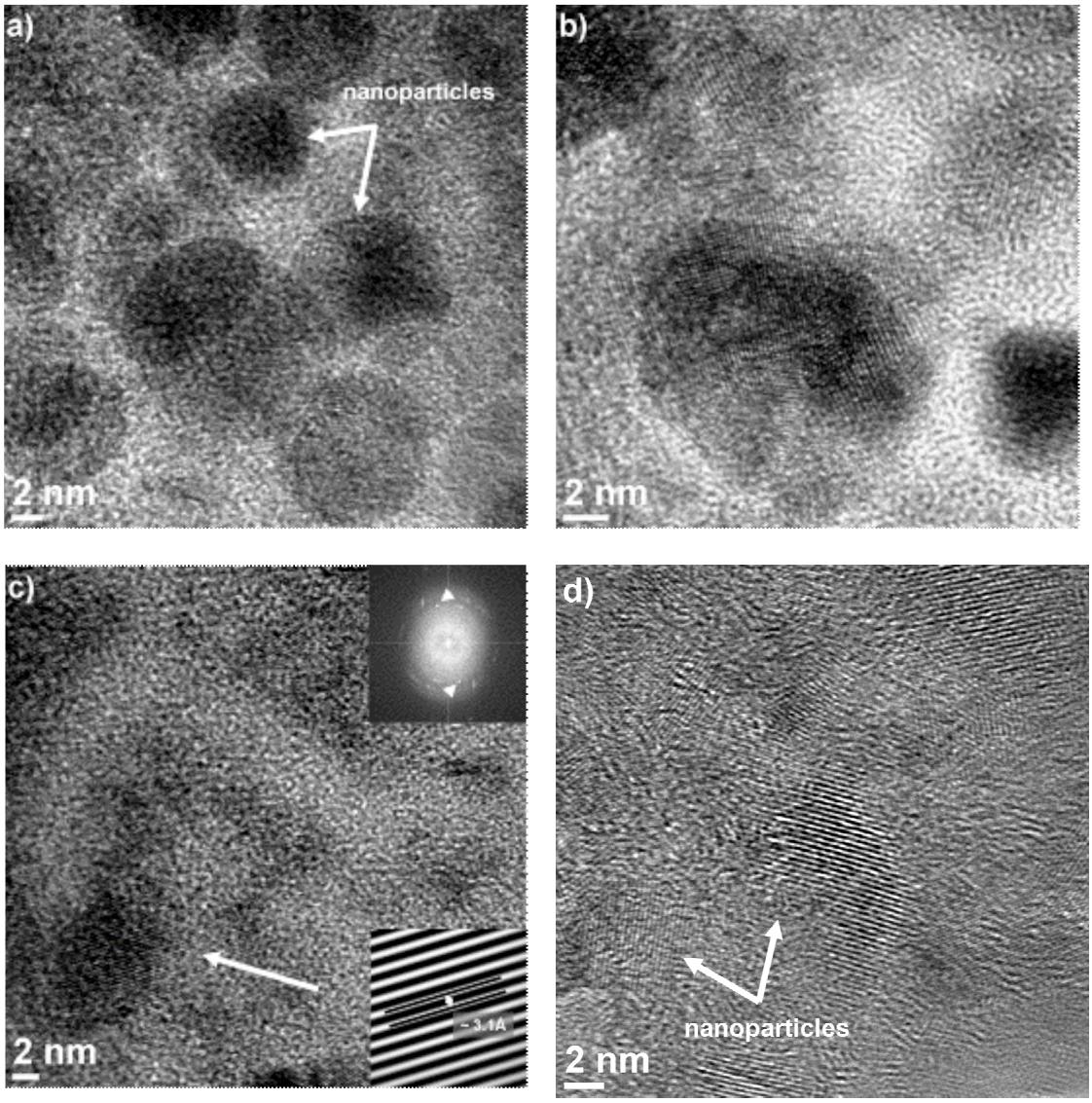

Figure S7. HRTEM images of a-c) PentaPAA27-5, and d) PentaPAA36-5 . The upper and lower insets show the FFT patterns and filtered inverse-FFT images, respectively. Calcium phosphate nanocrystals with sizes on the order of 5-10 nm were observed in PentaPAA27-5 sample. The existence of brushite was confirmed in PentaPAA27-5. Moreover, the analysis of c) showed that hydroxyapatite might also be present in PentaPAA27-5, consistent with NMR.

Additional References

29. Wanka, G.; Hoffmann, H.; Ulbricht, W. Macromolecules 1994, 27, 4145-4149.

30. Petrov, A. I.; Antipov, A. A.; Sukhorukov, G. B. Macromolecules 2003, 36, 10079-10086.

31. Chen, Q.; Schmidt-Rohr, K. Solid State NMR 2006, 29, 142-152.

32. Clauss, J.; Schmidt-Rohr, K.; Spiess, H. W. Acta Polymer. 1993, 44, 1-17.